A Spatial Fuzzy Clustering Algorithm With Kernel Metric Based on Immune Clone for SAR Image Segmentation

Ronghua Shang, *Member, IEEE*, Pingping Tian, Licheng Jiao, *Senior Member, IEEE*, Rustam Stolkin, *Member, IEEE*, Jie Feng, Biao Hou, *Member, IEEE*, and Xiangrong Zhang, *Member, IEEE*

***Abstract*—The fuzzy c-means (FCM) clustering algorithm has been widely used in image segmentation. However, FCM exhibits poor robustness to noise, often leading to unsatisfactory segmentations on noisy images. Additionally, the FCM algorithm is sensitive to the choice of initial cluster centers. In order to solve these problems, this paper proposes clone kernel spatial FCM (CKS_FCM), which improves segmentation performance in several ways. First, in CKS_FCM, an immune clone algorithm is used to generate the initial cluster centers, which helps prevent the algorithm from converging on local optima. Second, CKS_FCM improves the robustness to noise by incorporating spatial information into the objective function of FCM. Third, CKS_FCM uses a non-Euclidean distance based on a kernels metric, instead of the Euclidean distance conventionally used in FCM, to enhance the segmentation accuracy (SA). We present experimental results on both real and synthetic SAR images, which suggest that the proposed method can generate higher accuracy, and obtain more robustness to noise, as compared against six state-of-the-art methods from the literatures.**

***Index Terms*—Fuzzy C-means (FCM) cluster, immune clone algorithm, kernels metric, spatial information.**

I. Introduction

SYNTHETIC aperture radar (SAR) image segmentation is the process of partitioning an SAR image into several different spatial regions, such that the pixels within each such region share similar characteristics, but are different between regions [1]. SAR Image segmentation plays a key role in environmental monitoring and civil applications [2]. The result of image segmentation directly affects the quality of subsequent image analysis. Methods for quickly and effectively dividing the target area of interest from a complex background are therefore of significant interest [3]. SAR image segmentation algorithms have been researched for several decades, and a large number of different image segmentation methods have been proposed. These methods include threshold method [4], [5], region split and merge [6]–[8], model [9], [10], level set [11], [12], clustering [13]–[16], and others. Fuzzy theory has proved to be a useful way of handling image uncertainty and has, therefore, been widely applied to image segmentation. One of the most successful and popular methods in the literature is the fuzzy c-means (FCM) algorithm. FCM algorithm performs unsupervised clustering without needing human supervision, making it suitable for automatically segmenting images under conditions of fuzziness and uncertainty [17].

FCM is a nonlinear iterative optimization algorithm based on an objective function [18]. The objective function of FCM is a weighted similarity measure for each pixel of the image and the cluster centers [19]. The algorithm for image segmentation minimizes the objective function by iteration to choose appropriate cluster centers and membership degree matrix [20]. After the convergence, the segmented image can be obtained by using the membership and centers [21]. However, FCM often overlooks the spatial information of the image and uses Euclidean distance, often resulting in low segmentation accuracy (SA) and poor robustness to noise [13].

Many improved FCM algorithms have been proposed to try and exploit spatial information from the image. Ahmed *et al.* [22] proposed FCM_S, which introduced a spatial information term into the objective function. In this algorithm, the neighborhood term is computed in each iteration step, so the time complexity is high. In order to solve this problem of FCM_S, Chen *et al.* [23] proposed FCM_S1 and FCM_S2. FCM_S1 and FCM_S2 modified the objective function by introducing mean and median filtering terms, respectively, instead of the neighborhood term. The time complexity of FCM_S1 and FCM_S2 algorithm was reduced because the mean and median filtered images can be calculated in advance. To improve the speed of the clustering algorithm, Szilayi *et al.* [24] proposed the EnFCM algorithm, which formed a linear weighted image from the original image and the mean filtering image and used the histogram of the weighted image instead of pixels, thereby reducing computational complexity. Cai *et al.* [25] proposed a fast FCM (FGFCM) algorithm, which introduced similarity between pixels [26] to form a nonlinearly weighted image.

When the noise of the image is large, the neighborhood information may also contain abnormal features. So the nonlocal information is utilized in improved FCM algorithms. LNFCM [27], FCM_NLS [28], and FCA_NLASC [29] incorporate the

Manuscript received May 16, 2015; revised December 05, 2015; accepted January 03, 2016. Date of publication February 15, 2016; date of current version March 11, 2016. This work was supported in part by the National Natural Science Foundation of China, under Grant 61371201, Grant 61501353, and Grant 61271302, in part by the Program for New Century Excellent Talents in University under Grant NCET-12-0920, in part by the Program for New Scientific and Technological Star of Shaanxi Province under Grant 2014KJXX-45.

R. Shang, P. Tian, L. Jiao, J. Feng, B. Hou and X. Zhang are with the Key Laboratory of Intelligent Perception and Image Understanding of Ministry of Education, Xidian University, Xi'an 710071, China.

R. Stolkin is with the School of Mechanical Engineering, University of Birmingham, Birmingham B15 2TT, U.K. (e-mail: rhshang@mail.xidian.edu.cn).

Color versions of one or more of the figures in this paper are available online at http://ieeexplore.ieee.org.

Digital Object Identifier 10.1109/JSTARS.2016.2516014

nonlocal spatial information into FCM, respectively. All of these algorithms have been applied to noisy images, but the filtering degree parameter is hard to choose when the level of noise in an image is unclear. Jian *et al.* proposed NS_FCM [30]. This method improved a nonlocal means, including a new distance measure and an adaptive filtering degree parameter. NS_FCM also introduced between-cluster variation [31] into the objective function so that the robustness of the algorithm is increased.

The above-mentioned algorithms can achieve promising results on synthetic images, natural images, and medical images. However, when dealing with SAR images, they often generate unsatisfactory results. Furthermore, they may generate poor segmentation performance for images, which contain a lot of noise and some very similar classes. In addition, they are sensitive to the initial choice of cluster centers and prone to local optima convergence. Therefore, the automatic segmentation of SAR images using clustering algorithms remains a challenging problem. Our motivation is to try to solve these problems.

This paper proposes a spatial fuzzy clustering algorithm with kernel metric based on immune clone (CKS_FCM). It first uses the immune clone to get the initial cluster centers, which can reduce the likelihood of FCM converging on local optima. Then, we propose the improved nonlocal means filter in which the filter parameter is adjusted according to the noise. We introduce between-cluster variation and a nonlocal spatial information term into the objective function, which are obtained by the improved nonlocal means filter. By introducing these two terms, CKS_FCM utilizes nonlocal spatial information to reduce the effects of the noise and it considers both the compactness and the separation of the clustering results. So, CKS_FCM can adjust the distance between the cluster centers flexibly. Next, we use a non-Euclidean kernel-based distance in CKS_FCM, instead of the conventional Euclidean distance used in FCM. Clustering algorithms based on the non-Euclidean distance have been shown to be robust to outliers and noise [32]. Therefore, CKS_FCM is able to generate high SA and is more robustness to noise and outliers. The differences between the proposed method and the previously methods are summarized as follows. In CKS_FCM, the nonlocal spatial information term is introduced into FCM. The difference between the previously proposed FCM algorithms (e.g., LNFCM, FCM_NLS, and FCA_NLASC) is that the nonlocal spatial information in the CKS_FCM is obtained by the improved nonlocal means. The improved nonlocal means is proposed in this paper by using the adjustable filter parameter. The improved nonlocal means obtains the filter parameter according to the noise of the image and gets more reasonable result. The between-cluster variation term is introduced in CKS_FCM which is inspired by NS_FCM. By introducing the between cluster variation term, CKS_FCM considers both the compactness and the separation of the clustering results.

This paper is organized as follows. Section II introduces the CKS_FCM algorithm in detail. Section III describes empirical experiments on synthetic SAR images, real SAR images. Section IV provides concluding remarks.

II. Proposed Algorithm

A. Motivation and Notation

In conventional FCM, if the initial cluster centers are close to the final cluster centers, the number of iteration will be less, the amount of computation will be small and the convergence of the algorithm will be fast. Therefore, it is crucial to produce the good initial cluster centers. Immune clone is an optimization algorithm that simulates the biological principle of acquired immune clone. It is stable and comparatively reliable for finding optimal solutions. Immune clone can overcome the weaknesses of FCM, which is sensitive to initial choices of cluster centers and is prone to convergence on local optimal. In view of these shortcomings, this paper obtains the initial cluster centers from the immune clone algorithm, and further optimizes them by using an improved FCM algorithm. The proposed method not only takes advantages of the global search ability of immune clone but also exploits the local search ability of FCM. Hence, the clustering results are more reliable and image segmentation quality is significantly improved.

This paper also introduces a mean filtering term and a between-cluster separation term into the objective function of the FCM algorithm. Nonlocal image information is encoded in the mean filtering image term so that it can reduce the impact of noise on the original image. The between-cluster separation term can effectively solve the problem that FCM only considers compactness within cluster and ignores separation distance between clusters. Using non-Euclidean distance based on a Gaussian kernel, instead of the Euclidean distance of the conventional FCM algorithm, the proposed method can significantly improve SA and robustness against image noise.

The notation is summarized as follows. In immune clone, $\boldsymbol{a}_i(t)$ denotes the antibody, $\boldsymbol{A}_1(t)$ denotes the initial antibody groups, $\boldsymbol{A}_2(t)$ denotes the cloning antibody groups, $\boldsymbol{A}_3(t)$ denotes the mutation antibody groups, p_m denotes the mutation probability, and N_C denotes the number of clones. In improved nonlocal means, r denotes the radius of the nonlocal search window. $\overline{x}_i$ denotes the nonlocal weighted mean. In improved FCM, N denotes the number of pixels in the image, c is the number of clusters and u_{ki} is the membership degree of pixel x_i belonging to the cluster k. Parameter m is a weighting exponent on each fuzzy membership and x_i denotes the pixels of the original image. G_{ki} is a fuzzy factor, $k(x_i, V_k)$ denotes the non-Euclidean distance.

B. Image Clustering Procedure

The basic framework of CKS_FCM can be divided into three parts: initialization of cluster centers; image filtering based on improved nonlocal means; and iteration of CKS_FCM.

1) Initialize Cluster Centers: The initial cluster centers must be given in FCM. FCM is sensitive to the choice of initial cluster center positions, and is prone to local minima convergence. The immune clone algorithm [33] can help overcome these weaknesses of FCM. The main steps of immune clone algorithm [34] adapted for CKS_FCM are as follows.

a) Antibody encode: In CKS_FCM, we encode the antibody based on the clustering center as genes by floating-point.

$\boldsymbol{x}_{i1}(t)$	$\boldsymbol{x}_{i2}(t)$	...	$\boldsymbol{x}_{ik}(t)$	$\boldsymbol{x}_{ik+1}(t)$	...	$\boldsymbol{x}_{ic}(t)$

Fig. 1. form of antibody $\boldsymbol{a}_i(t)$.

TABLE I
CLONE OPERATOR FOR INITIALIZING CLUSTER CENTERS

Algorithm 1: process of clone operator
Input: Initial antibody groups $A_1(t)$, the number of cloning;
Output: Cloning antibody groups $A_2(t)$;
Begin
1. Calculate the affinity $A_{f1}(A_1(t))$ of the initial antibody groups $A_1(t)$;
2. Sort the affinity $A_{f1}(A_1(t))$ to get $A_{f2}(A_1(t))$;
3. Choose top 0.5*N of $A_{f2}(A_1(t))$ best antibodies for N_{C1} number of cloning;
4. Choose other antibodies for N_{C2} number of cloning;
5. Output the new antibody groups $A_2(t)$.

End

The image pixels are encoded as samples and the number of the samples is n. Then, we randomly select c samples as initial cluster centers and these samples are cascaded to form an antibody vector $\boldsymbol{a}_i(0)$. By repeating this process N times to get N antibodies, we obtain the initial antibody groups $\boldsymbol{A}_1(0)$. Then, the antibody groups of the tth generation are $\boldsymbol{A}_1(t) = \{\boldsymbol{a}_1(t), \boldsymbol{a}_2(t), \ldots, \boldsymbol{a}_i(t), \ldots, \boldsymbol{a}_N(t)\}$ and $\boldsymbol{a}_i(t)$ denotes the antibody. Antibody $\boldsymbol{a}_i(t)$ is shown in Fig. 1, where the $\boldsymbol{x}_{i1}(t)$ denotes the genes.

b) Affinity: In CKS_FCM, affinity is defined in terms of the objective function of the FCM. For each antibody $\boldsymbol{a}_i(t)$, the affinity is calculated as follows:

$$A_f(\boldsymbol{a}_i(t)) = 1/\left(1 + J_{FCM}(U, V)\right). \tag{1}$$

$J_{FCM}(U, V)$ is the objective function of the FCM algorithm. The smaller the objective function, the closer the cluster centers will be to the globally optimal cluster centers.

c) Clone operator: In this paper, the antibody clone operator is based on antibody affinity. The larger the values for antibody affinity, the closer the cluster centers of the antibody become to the optimal cluster centers. Therefore, we should choose the antibody with largest affinity for cloning. The affinity of the antibody groups is calculated and sorted. Then, we choose the best antibodies of the top 20% sorting affinity for N_{C1} number of cloning and other 20%–40% antibodies for N_{C2} number of cloning. After the cloning, we obtain the new cloning antibody groups $\boldsymbol{A}_2(t)$. The procedure for the clone operator used in CKS_FCM is shown in Table I.

d) Immune operator: For each antibody of the cloning antibody groups $\boldsymbol{A}_2(t)$, the immune operator used in CKS_FCM randomly generates an integer n between 1 and c, which indicates the position of mutation. Then, it randomly generates a number p between 0 and 1. If p is less than mutation probability p_m, it will use the other random samples to replace the nth gene in the antibody $\boldsymbol{a}_i(t)$. By the immune operator, we get the mutation antibody groups $\boldsymbol{A}_3(t)$. The process is shown in Table II.

In summary, the process of initializing cluster centers is shown in Table III.

The flowchart for initializing cluster centers by immune clone is shown in Fig. 2.

2) Image Filtering Based on Improved Nonlocal Means: FCM considers the image gray value features, but does not take into account the image spatial information, which leads to discontinuities within the segmented image regions. In order to improve the quality of image segmentation, we should also consider spatial characteristics of the image.

TABLE II
IMMUNE OPERATOR FOR INITIALIZING CLUSTER CENTERS

Algorithm 2: the process of immune operator
Input: cloning antibody groups $A_2(t)$, mutation probability p_m;
Output: mutation antibody groups $A_3(t)$;
Begin
1. Each antibody for cloning antibody groups $A_2(t)$, randomly generate a number p between 0 and 1;
2. **If** $p<p_m$
3. n=rand(1, c), use the other random genetic of the samples to replace the n-th genes in the antibody;
   End
4. Output the new antibody groups $A_3(t)$.

End

TABLE III
PROCESS FOR INITIALIZING CLUSTER CENTER

Algorithm 3: The process for initializing cluster centers using immune clone
Input: original image I, mutation probability p_m=0.6, the number of cloning N_{C1}=6, N_{C2}=5;
Output: initial clustering centers V_1;
Begin
1. The pixels is encoded to obtain the initial antibody groups $A_1(0)$ and set the maximum number of iterations G_{max};
2. **While** ($t<G_{max}$)
3. t=1,
4. clone operator for initial antibody groups $A_1(t)$ to get cloning antibody groups $A_2(t)$;
5. Immune operator for cloning antibody groups $A_2(t)$ to get mutation antibody groups $A_3(t)$;
6. Calculate the affinity of the antibody groups A1(t) and A3(t) and sort them, then update the antibody groups $A_1(t)$ by choosing top N antibodies in $A_1(t)$, $A_2(t)$and $A_3(t)$;
7. t=t+1;
8. **end while**
9. Decode the best antibody to obtain the initial cluster centers V_1.

End

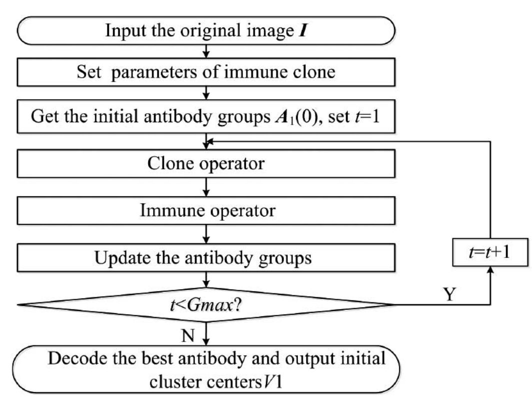

Fig. 2. Flowchart of initialization cluster centers.

The pixels in the nonlocal window around the center pixel generally have the same characteristics, we can get nonlocal mean of the pixels in the nonlocal window of the pixel by these same characteristics. Here, the "nonlocal mean" means the mean value of the pixels in the nonlocal window. The nonlocal means (NL-means) algorithm for image denoising is proposed by Buades *et al.* [35], [36].

The filter parameter of NL-means has a significant influence on the filter result. We cannot obtain ideal results if the filter parameter h is too small or too large. Too large h will cause the over-smoothing result and damage the image information. Too small h causes the under-smoothing result and the noises exist in the image. Therefore, the parameter should be adjusted according to the nonlocal information of the image. If the noise in the image is serious, the parameter h will be large, and vice versa. In the proposed algorithm, we use an adjustable filter parameter instead of the fixed values that are conventionally employed in NL-means.

For each pixel x_i in the image, the adjustable filter parameter h_i is calculated by the following formula

$$h_i = \frac{1}{r^2 - 1} \sum_{j=1}^{r^2} \|v(N_i) - v(N_j)\|_{2,\sigma}^2, j \in N_i \tag{2}$$

where $\sigma > 0$ is the standard deviation of the Gaussian kernel, $v(N_i) = \{x_j, x_j \in N_i\}$ is the element within the nonlocal search window, r is the radius of the nonlocal search window size.

This paper obtains a filtered image I_m by using the improved NL-means. It calculates the nonlocal weighted mean of each pixel in the nonlocal search window. For each pixel x_i in the image, we first generate a nonlocal search window of radius r and then calculate the similarity between the center pixel x_i and pixel x_j in the search windows. The formula for computing the similarity is as follows:

$$S_{ij} = \|v(N_i) - v(N_j)\|_{2,\sigma}^2. \tag{3}$$

Then, we calculate weight w_{ij} of pixel x_j in the search window by using the similarity s_{ij} usingthe following formula

$$w_{ij} = \frac{1}{Z_j} \exp\left(-S_{ij} \Big/ h_i\right) \tag{4}$$

where Z_j is the normalizing parameter, h_i is the adjustable filtering parameters. The Z_j is defined as follows:

$$Z_j = \sum_{j \in N_i} \exp\left(-s_{ij} \Big/ h_i\right). \tag{5}$$

Finally, we calculate the nonlocal weighted mean of each pixel by using the weight w_{ij}, with the formula

$$\overline{x}_i = \sum_{j \in N_i} w_{ij} x_j \tag{6}$$

where $\overline{x}_i$ denotes the nonlocal weighted mean and N_i denotes the nonlocal search window of radius r. In summary, the improved nonlocal means algorithm is shown in Table IV.

The flowchart of the improved nonlocal means is shown in Fig. 3. The additional steps of the nonlocal means algorithm (beyond conventional methods) are indicated by a broken line.

3) General Framework of CKS_FCM Iteration: The nonlocal spatial information term and between-cluster variation term are introduced into the objective function. Then, a non-Euclidean distance based on kernel is used in CKS_FCM instead of the Euclidean distance used in FCM.

TABLE IV
PROCESS OF IMPROVED NONLOCAL MEANS FOR FILTERING IMAGE

Algorithm 4: The process of the improved non-local means for filtering image
Input: The original image I;
Output: The filtering image I_m;
Begin
[m, n]=size(I);
for i=1: m
  for j=1: n
    For each pixel $x(i, j)$, get the non-local search window of radius r;
    Calculate the weight $w_{(i,j)(p,q)}$ of the pixels $x(p, q)$ within the search Window using the adjustable filter parameter h_i;
    Calculate the non-local weighted mean $\overline{x}(i, j)$;
  end for
end for
End

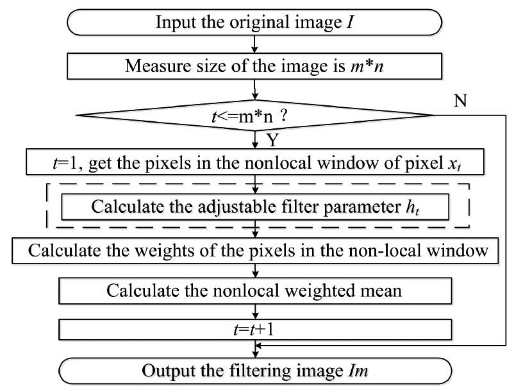

Fig. 3. Flowchart of the improved nonlocal means algorithm.

a) Objective function of CKS_FCM: The objective function of CKS_FCM is defined as follows:

$$\begin{aligned} J_m(U,V) = &\sum_{i=1}^{n}\sum_{k=1}^{c} u_{ki}^m \|\Phi(x_i) - \Phi(V_k)\|^2 \\ &+ \alpha \sum_{i=1}^{n}\sum_{k=1}^{c} u_{ki}^m \|\Phi(\overline{x}_i) - \Phi(V_k)\|^2 \\ &- n(k) \sum_{i=1}^{n}\sum_{k=1}^{c} u_{ki}^m \|\Phi(\overline{x}) - \Phi(V_k)\|^2 + G_{ki} \end{aligned} \tag{7}$$

where n is the number of pixels in the image, c is the number of clusters, and u_{ki} is the membership degree of pixel x_i belonging to the cluster k. Parameter m is a weighting exponent on each fuzzy membership and x_i denotes the pixels of the original image. G_{ki} is a fuzzy factor [37], which uses the non-Euclidean distance. $\|\Phi(\overline{x}_i) - \Phi(V_k)\|^2$ is the mean filtering term and $\overline{x}_i$ denotes the pixels of the filtered image generated by the improved nonlocal means algorithm. Parameter a controls the effect of the mean filtering term. $\|\Phi(\overline{x}) - \Phi(V_k)\|^2$ is the between-cluster variation term and $\overline{x}$ denotes the mean of all pixels of the original image. Parameter $n(k)$ controls the effect of the between-cluster separation term and is calculated as

$$n(k) = \frac{(b/4)\min_{k' \neq k}\|v(k) - v(k')\|^2}{\max_j \|v_j - \overline{x}\|^2}. \tag{8}$$

$\|\bullet\|$ denotes the Euclidean norm and Φ is an implicit nonlinear map [38] in the feature space and the inner product between

$\Phi(x_i)$ and $\Phi(V_k)$ is $\Phi(x_i)^T\Phi(V_k) = K(x_i, V_k)$. Through the kernel replacement, we can get

$$\begin{aligned}
&\|\Phi(x_i) - \Phi(V_k)\|^2 \\
&= (\Phi(x_i) - \Phi(V_k))^T(\Phi(x_i) - \Phi(V_k)) \\
&= \Phi(x_i)^T\Phi(x_i) - \Phi(V_k)^T\Phi(x_i) - 2\Phi(x_i)^T\Phi(V_k) \\
&= K(x_i, x_i) + K(V_k, V_k) - 2K(x_i, V_k) = 2(1 - K(x_i, V_k)).
\end{aligned} \tag{9}$$

In this way, the non-Euclidean distance based on kernels in the original data is obtained. For simplicity, we select a Gaussian radial basis kernel function (GRBF). Kernel distance based on the Gaussian kernel is defined as follows:

$$K(x_i, V_k) = \exp\left(\frac{-\|x_i - V_k\|^2}{\sigma}\right) \tag{10}$$

where σ is the bandwidth of the GRBF. The parameter σ is set on the basis of the distance of all pixels, which is similar to the work of [39]. Let $dis_i = \|x_i - \overline{x}\|$ be the distance from pixel x_i to the pixels average $\overline{x}$. The mean distance of dis_i is calculated as follows:

$$\overline{dis} = \frac{\sum_{i=1}^{n} dis_i}{n}. \tag{11}$$

Then, we can get σ as follows:

$$\sigma = \left(\frac{1}{n-1}\sum_{i=1}^{n}(dis_i - \overline{dis})^2\right)^{0.5}. \tag{12}$$

Thus, the objective function of CKS_FCM with non-Euclidean distance based on the Gaussian kernel is given as follows:

$$\begin{aligned}
J_m(U, V) = &\sum_{i=1}^{n}\sum_{k=1}^{c} u_{ki}^m(1 - K(x_i, V_k)) \\
&+ \alpha\sum_{i=1}^{n}\sum_{k=1}^{c} u_{ki}^m(1 - K(\overline{x}_i, V_k)) \\
&- n(k)\sum_{i=1}^{n}\sum_{k=1}^{c} u_{ki}^m(1 - K(\overline{x}, V_k)) + G_{ki}.
\end{aligned} \tag{13}$$

In (13), the fuzzy factor G_{ki} is written as follows:

$$\begin{aligned}
G_{ki} &= \sum_{j\in N_i, i\neq j}\frac{1}{1 + d_{ij}}(1 - u_{kj})^m\|\Phi(x_i) - \Phi(V_k)\|^2 \\
&= \sum_{j\in N_i, i\neq j}\frac{1}{1 + d_{ij}}(1 - u_{kj})^m(1 - K(x_i, V_k))
\end{aligned} \tag{14}$$

where N_i is a neighborhood window of radius t with respect to the center pixel i, d_{ij} is Euclidean distance between center pixel i and pixel j in the neighborhood window N_i. u_{kj} is membership degree.

b) Iterative formula of CKS_FCM: According to the above process, the objective function of the proposed algorithm is obtained. We obtain the updating formula of membership degree and cluster centers by minimizing the objective function of CKS_FCM by using Lagrange multipliers as follows.

We define a new objective function with constraint condition (15) as follows:

$$\begin{aligned}
L_m = &\sum_{i=1}^{n}\sum_{k=1}^{c} u_{ki}^m(1 - K(x_i, V_k)) \\
&+ \alpha\sum_{i=1}^{n}\sum_{k=1}^{c} u_{ki}^m(1 - K(\overline{x}_i, V_k)) \\
&- n(k)\sum_{i=1}^{n}\sum_{k=1}^{c} u_{ki}^m(1 - K(\overline{x}, V_k)) + G_{ki} \\
&+ \sum_{i=1}^{n}\lambda\left(1 - \sum_{k=1}^{c} u_{ki}\right).
\end{aligned} \tag{15}$$

Next, we derive the partial derivative of L_m with respect to u_{ki} and λ, and then set the partial derivative to equal to zero

$$\frac{\partial L_m}{\partial u_{ki}} = m{u_{ki}}^{m-1}((1 - K(x_i, V_k)) + \alpha(1 - K(\overline{x}_i, V_k)) \tag{16}$$

$$-n(k)(1 - K(\overline{x}, V_k)) + G_{ki}) - \lambda = 0$$

$$\frac{\partial L_m}{\partial \lambda} = \sum_{k=1}^{c} u_{ki} - 1 = 0. \tag{17}$$

From equation (16), we can get

$$u_{ki} = \left(\frac{\lambda}{\begin{gathered}m((1 - K(x_i, V_k)) + \alpha(1 - K(\overline{x}_i, V_k)) \\ -n(k)(1 - K(\overline{x}, V_k)) + G_{ki})\end{gathered}}\right)^{\frac{1}{m-1}}. \tag{18}$$

Substituting (17) into (18), we obtain

$$\left(\frac{\lambda}{m}\right)^{\frac{1}{m-1}}\sum_{j=1}^{c}\left(\frac{1}{\begin{gathered}(1 - K(x_i, V_j)) + \alpha(1 - K(\overline{x}_i, V_j)) \\ -n(k)(1 - K(\overline{x}, V_j)) + G_{ji}\end{gathered}}\right)^{\frac{1}{m-1}} = 1. \tag{19}$$

Therefore,

$$\left(\frac{\lambda}{m}\right)^{\frac{1}{m-1}} = \left(\frac{1}{\sum_{j=1}^{c}\left(\begin{gathered}(1 - K(x_i, V_j)) + \alpha(1 - K(\overline{x}_i, V_j)) \\ -n(k)(1 - K(\overline{x}, V_j)) + G_{ji}\end{gathered}\right)}\right)^{\frac{-1}{m-1}}. \tag{20}$$

Finally, substituting (20) into (18), we can get the membership degree in (21), shown at the bottom of the page.

Similarly, we obtain the partial derivative of L_m with respect to V_k

$$\frac{\partial Lm}{\partial Vk} = \sum_{i=1}^{n} u_{ki}{}^{m} \left(\begin{array}{c} K(x_i, V_k)\frac{2(x_i - V_k)}{\sigma} + \alpha K(\overline{x}_i, V_k)\frac{2(\overline{x}_i - V_k)}{\sigma} \\ -n(k)K(\overline{x}, V_k)\frac{2(\overline{x} - V_k)}{\sigma} \end{array} \right) = 0. \tag{22}$$

From (22), we have

$$\sum_{i=1}^{n} u_{ki}{}^{m} \left(K(x_i, V_k)x_i + \alpha K(\overline{x}_i, V_k)\overline{x}_i - n(k)K(\overline{x}, V_k)\overline{x} \right) = \sum_{i=1}^{n} u_{ki}{}^{m} \left(K(x_i, V_k) + \alpha K(\overline{x}_i, V_k) - n(k)K(\overline{x}, V_k) \right) V_k. \tag{23}$$

Finally, we get the cluster center as follows:

$$V_k = \frac{\sum_{i=1}^{n} u_{ki}{}^{m}(K(x_i, V_k)x_i + \alpha K(\overline{x}_i, V_k)\overline{x}_i - n(k)K(\overline{x}, V_k)\overline{x})}{\sum_{i=1}^{n} u_{ki}{}^{m} \left(K(x_i, V_k) + \alpha K(\overline{x}_i, V_k) - n(k)K(\overline{x}, V_k) \right)}. \tag{24}$$

The CKS_FCM algorithm constantly updates its membership matrix and cluster centers by using the membership degree formula (21), shown at the bottom of the page, and cluster centers formula (24). It will not stop until the difference between the new cluster centers and the last cluster centers is less than the stop condition. Once the algorithm has converged, we can generate the segmented image by using the final membership degree and cluster centers.

c) Key steps of the CKS_FCM algorithm: The important steps of the spatial fuzzy clustering algorithm with kernel metric based on immune clone for SAR image segmentation (CKS_FCM) are: first use the immune clone algorithm to generate global initial cluster centers; then uses the improved nonlocal means algorithm to obtain filtered images; finally use (21) and (24) to update membership degree and cluster centers. The overall algorithm process is shown in Table V.

The overall flowchart of the proposed algorithm CKS_FCM is shown in Fig. 4.

TABLE V
PROCESS OF CKS_FCM

Algorithm 5: The process of CKS_FCM
Input: The original image *I*;
Output: Segmented image I_s, cluster center V_2, membership degree U_{ki};
Begin
1. Input the image *I*, measure the size of the image and convert it to gray images, then set the parameters of FCM: number of cluster center *c*, threshold *e*, the fuzzy parameter *m*, the maximum number of iterations T_{max}, the radius of non-local search window and neighbors window;
2. Get the global optimal initial clustering center V_1 by immune clone algorithm;
3. Get the filtering image I_m by improved NL-means algorithm;
4. Set the loop counter t=1;
5. Randomly initialize the membership degree;
6. **While** ($t<T_{max}$)
7. Update the membership degree matrix U_{ki} using(12);
8. Update the cluster center V_2 using(13);
9. If max $|V2-V1|<e$, then stop and output the membership degree U_{ki} and new cluster Center V_2; Otherwise, set loop counter t=t+1and go to(7);
10. **End while**
11. Get segmented image I_s from new cluster centers V_2 and membership degree U_{ki}.
End

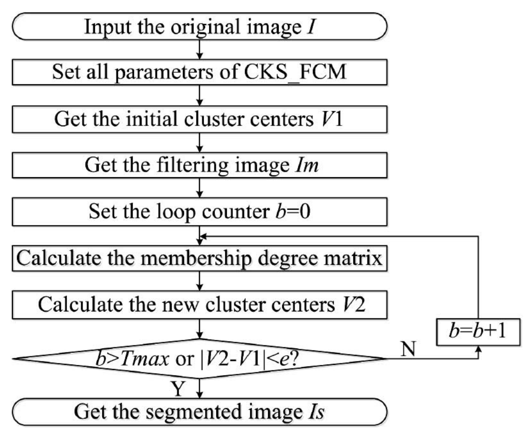

Fig. 4. Flowchart of CKS_FCM.

III. EXPERIMENTAL RESULTS

A. Experimental Data

In this paper, two synthetic SAR images and two real SAR images are included in the experiment. They are shown in Fig. 5. The size of the first synthetic image is 244×244. The ground-truth pixels of the synthetic image comprise four different image regions, with pixel intensity values 0, 85, 170, and 255 respectively, as shown in Fig. 5(a). The size of the second synthetic image is 256×256, as shown in Fig. 5(b). The synthetic SAR images are contaminated with different noise. The type of noise is different-level fully developed speckle noise. Numbers of looks are 1, 2, 4, and 6 [40]. The first real SAR image is a VV polarization, four-look European remote sensing satellite (ERS-2) image with 12.5-m resolution near Rome, Italy, shown in Fig. 5(c). It can be divided into three types of crops. The second real SAR image is an airborne X-band, eight-look image with 1-m resolution near Xi'an, China [13]. It can be divided into four types of land covers: three types of crops and water, shown in Fig. 5(d).

$$u_{ki} = \frac{\sum_{j=1}^{c} ((1 - k(x_i, V_j)) + \alpha(1 - k(\overline{x}_i, V_j) - n((k)(1 - k(\overline{x}, V_j) + G_{ji})^{\frac{1}{m-1}}}{((1 - k(x_i, V_k)) + \alpha(1 - k(\overline{x_i}, V_k) - n((k)(1 - k(\overline{x}, V_k) + G_{ki})^{\frac{1}{m-1}}}. \tag{21}$$

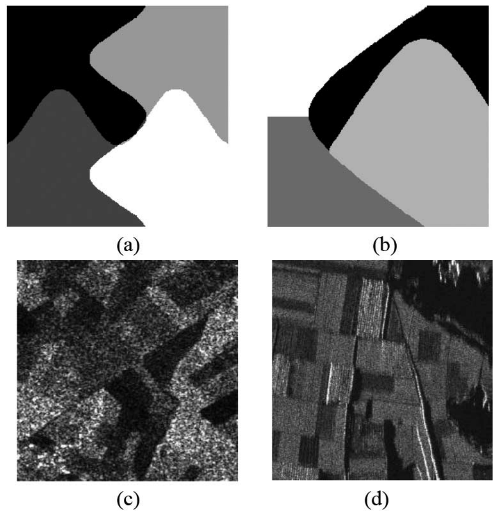

Fig. 5. Experimental data.

B. Evaluation Indexes

In this paper, we use the SA, partition coefficient v_{pc} and partition entropy v_{pe} as the evaluation indices. SA is defined as the sum of correctly classified pixels divided by the total number of pixels [41]

$$SA = \sum_{i=1}^{c} \frac{A_i \cap C_i}{\sum_{j=1}^{c} C_j} \tag{25}$$

where c is the number of clusters, A_i denotes the pixels belonging to the $i\mathrm{th}$ class found by algorithm, and C_i denotes the pixels belonging to the $i\mathrm{th}$ class in the reference segmented image.

Partition coefficient v_{pc} and partition entropy v_{pe} [42] are defined as

$$v_{pc} = \frac{\sum_{i=1}^{n} \sum_{k=1}^{c} u_{ki}^2}{n} \tag{26}$$

$$v_{pe} = \frac{-\sum_{i=1}^{n} \sum_{k=1}^{c} (u_{ki} \log u_{ki})}{n} \tag{27}$$

where n is the number of pixels in the image, c is the number of clusters, and u_{ki} is the membership degree.

The best clustering result is achieved when SA approaches to1, v_{pc} approaches to1 and v_{pe} approaches to 0.

C. Performance Comparison of Algorithms and Parameter Analysis

In order to evaluate the efficiency of CKS_FCM, we use the FCM_S1 [21], FCM_S2 [21], KFCM_S1 [21], KFCM_S2 [21], FLICM [37], and NS_FCM [29] as the compared algorithms. For all algorithms, we set the fuzziness index $m = 2$, the threshold $e = 0.01$, the maximum iteration number $T_{max} = 500$, respectively. The radius of neighborhood for compared algorithms is 3. According to the literature [21], the parameter α is set to 5 for FCM_S1, FCM_S2, KFCM_S1, and KFCM_S2. The parameter α and β for NS_FCM are 5.5. The nonlocal mean search window is 11×11 for NS_FCM. The parameters uses in this method are analyzed as follows:

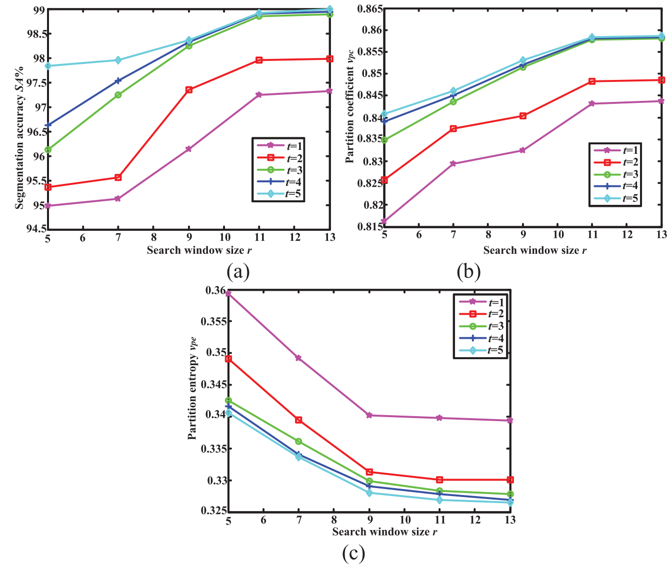

Fig. 6. SA values, the partition coefficient v_{pc}, and partition entropy v_{pe} of CKS_FCM with different size of window.

1) Size of Search Window and the Size of Neighborhood Window: The size of the nonlocal search window and the size of the neighborhood window are analyzed in this section. We investigate these two parameters on 4-look amplitude synthetic speckled image, which is shown in Fig. 5(a). The value of search window r changes from 5 to 13 with an interval of 1. The value of neighborhood window t changes from 1 to 5 with an interval of 1. The SA values, the partition coefficient v_{pc} and partition entropy v_{pe} of CKS_FCM with different radiuses are shown in Fig. 6.

It can be seen from Fig. 6 that the size of the nonlocal search window and the size of the neighborhood window affect the results. It is shown in Fig. 6(a) that with each r, the SA values are low when the neighborhood window t is 1 and 2. When t is larger than 3, the SA becomes higher. The curve of partition coefficient v_{pc} rises acutely with the increase of t from1 to 3. The curve of partition entropy v_{pe} reduces acutely with the increase of t from1 to 3. Moreover, with each t, the SA curve and partition coefficient v_{pc} ascend acutely with r from 5 to 11, and changes little with r is more than 11. The partition entropy v_{pe} reduces acutely with r from 5 to 9, and changes little with r is more than 9. So, we choose the size of neighborhood window $t = 3$, the size of nonlocal search window $r = 11$, considering the tradeoff between performance and computational cost.

2) Parameters a and b: Two free parameters a and b are analyzed in this section. Parameter a controls the effect of the mean filtering term and b is a part in $n(k)$, ****which controls the effect of the between-cluster separation term. We study these two parameters on the synthetic image 1 shown in Fig. 5(a). The 4-look amplitude synthetic speckled image is used for testing. The SA values, the partition coefficient v_{pc}, and partition entropy v_{pe} of CKS_FCM with different values of α and b are shown in Fig. 7.

It can be seen from Fig. 7(a) that the SA value increases significantly with the increase of α and b from 1 to 6. From Fig. 7(b), with the increase of both a and b from 1 to 6, the partition coefficient v_{pc} value increases. When a is 6 and b is

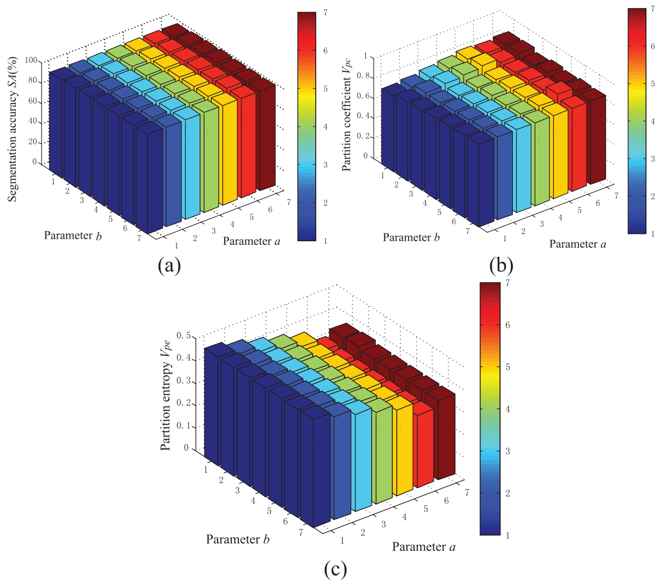

Fig. 7. *SA* values, the partition coefficient v_{pc}, and partition entropy v_{pe} of CKS_FCM with different *a* and *b*.

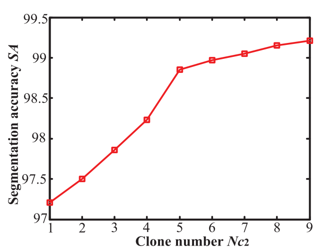

Fig. 8. *SA* values of CKS_FCM with different clone number N_{c_2}.

larger than 3, the value of partition coefficient v_{pc} reaches its maximum value. When a is larger than 6, the partition coefficient v_{pc} value begins to reduce. From Fig. 7(c), the value of partition entropy v_{pe} decreases significantly with the increase of a from 1 to 6. When a is larger than 6, the partition entropy v_{pe} begins to increase. Better clustering results correspond to larger *SA* values, larger partition coefficients, v_{pc} and smaller partition entropies v_{pe}. Hence, the key parameters setting are $a = 6$ and $b = 6$.

3) Parameters in Immune Clone: For CKS_FCM, we set the antibody groups size $N = 60$. The number of cloning N_{C2} and mutation probability p_m are analyzed in this part. We investigate these two parameters on the 4-look amplitude synthetic speckled image, which is shown in Fig. 5(a). The *SA* values of CKS_FCM with different clone number N_{C2} from 1 to 9 with an interval of 1 are shown in Fig. 8.

It can be seen from Fig. 8 that the *SA* value shows a sharp rise when N_{C2} increases from 1 to 5. When N_{C2} is larger than 6, the increase of SA values is not obvious. Larger cloning number needs higher computation cost. So we choose $N_{C2} = 5$. In CKS_FCM, the top 20% best antibodies are cloned with cloning number N_{C1} and other 20%–40% antibodies are cloned with cloning number N_{C2}. So we choose $N_{C1} = N_{C2} + 1$ so that the top 20% best antibodies can get more chance to survive.

The influence of mutation probability p_m to the performance of CKS_FCM is also analyzed. The curve is shown in Fig. 9,

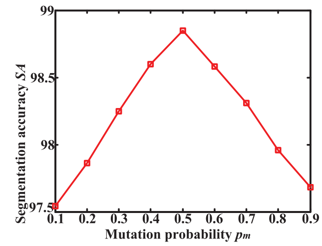

Fig. 9. *SA* values of CKS_FCM with different mutation probability p_m.

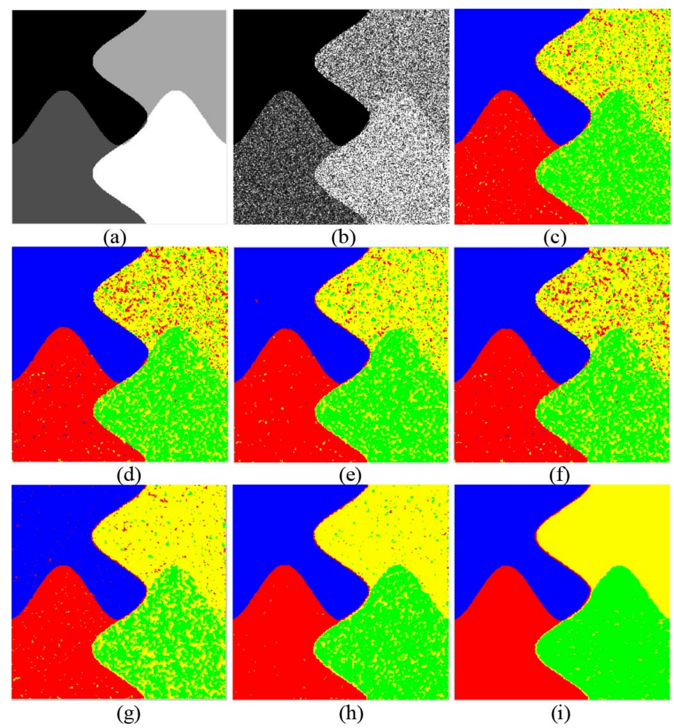

Fig. 10. Segmentation results on the 4-look amplitude synthetic speckled image. (a) Original image. (b) Noisy image. (c) FCM_S1 result. (d) FCM_S2 result. (e) KFCM_S1 result. (f) KFCM_S2 result. (g) FLICM result. (h) NS_FCM result. (i) CKS_FCM result.

where mutation probability p_m changes from 0.1 to 0.9 with an interval of 0.1.

It can be seen from Fig. 9 that SA value increases when the mutation probability p_m is less than 0.5 and decreases when p_m is larger than 0.5. So SA value gets the maximum value when $p_m = 0.5$. Hence, we set the mutation probability to be 0.5.

D. Results on Synthetic Images

The noise-free image is corrupted by speckle noise to generate the synthetically speckled image [43]. The *L*-look amplitude synthetic speckled image is contaminated with different-look fully developed speckle is used in the experiments, and the performance of algorithms is evaluated by SA, partition coefficient v_{pc}, and partition entropy v_{pe}. The speckle looks is arranged as 1, 2, 4, and 6.

The 4-look amplitude synthetic speckled image of size 244×244 is shown in Fig. 10(b). The segmentation results by the algorithms are shown in Fig. 10(c)–(i).

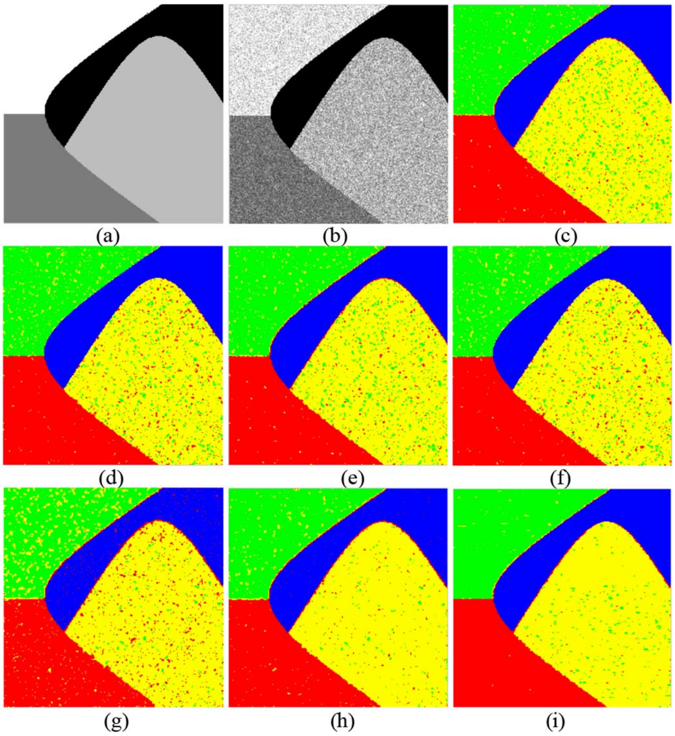

Fig. 11. Segmentation results on the 6-look amplitude synthetic speckled image. (a) Original image. (b) Noisy image. (c) FCM_S1 result. (d) FCM_S2 result. (e) KFCM_S1 result. (f) KFCM_S2 result. (g) FLICM result. (h) NS_FCM result. (i) CKS_FCM result.

TABLE VI
SEGMENTATION ACCURACY ($SA\%$) ON FIRST SYNTHETIC SPECKLED IMAGE

LOOKS	1	2	4	6
FCM_S1	70.65±0.31	78.65±0.41	86.40±0.61	89.91±0.27
FCM_S2	65.30±0.13	75.48±0.42	85.03±0.18	89.19±0.16
KFCM_S1	74.26±0.12	82.59±0.23	89.69±0.25	92.73±0.55
KFCM_S2	66.99±0.21	77.79±0.16	86.97±0.14	91.24±0.14
FLICM	72.06±0.14	79.47±0.46	89.44±0.19	70.65±0.28
NS_FCM	86.30±0.32	90.41±0.12	92.72±0.15	94.45±0.24
CKS_FCM	**92.70±1.51**	**97.26±1.76**	**98.85±1.14**	**99.04±0.46**

TABLE VII
SEGMENTATION ACCURACY ($SA\%$) ON SECOND SYNTHETIC SPECKLED IMAGE

LOOKS	1	2	4	6
FCM_S1	69.78±0.12	80.12±0.35	89.90±0.21	94.69±0.45
FCM_S2	68.38±0.16	79.56±0.17	89.69±0.24	94.70±0.52
KFCM_S1	72.24±0.45	81.61±0.46	90.45±0.35	94.61±0.36
KFCM_S2	68.74±0.43	79.79±0.47	90.20±0.68	94.97±0.56
FLICM	78.16±0.29	87.35±0.19	94.52±0.23	94.78±0.49
NS_FCM	74.02±0.24	86.36±0.32	92.74±0.46	94.52±0.86
CKS_FCM	**87.56±1.52**	**89.83±1.19**	**97.59±1.12**	**97.70±1.41**

TABLE VIII
v_{pc} AND v_{pe} ON FIRST SYNTHETIC SPECKLED IMAGE

INDEX	FCM_S1	FCM_S2	KFCM_S1	KFCM_S2	FLICM	NS_FCM	CKS_FCM
v_{pc}	0.7511 ±0.002	0.7639 ±0.001	0.7179 ±0.005	0.7372 ±0.005	0.7703 ±0.001	0.7985 ±0.005	**0.9522 ±0.165**
v_{pe}	0.4780 ±0.003	0.4568 ±0.009	0.5552 ±0.008	0.5916 ±0.009	0.4436 ±0.001	0.4009 ±0.006	**0.1567 ±0.158**

The segmentation results on the 4-look amplitude synthetic speckled image of FCM_S1 FCM_S2, KFCM_S1, and KFCM_S2 are shown in Fig. 10(c)–(f). Each segmented region is affected by noise seriously and the region uniformity is poor. The boundaries between the green and yellow regions are not well defined. The segmentation result of FLICM and NS_FCM is shown in Fig. 10(g) and (h). The misclassified points in the segmented image are less than the segmented images of FCM_S1, FCM_S2, KFCM_S1, and KFCM_S2. The segmentation result of CKS_FCM is shown in Fig. 10(i). The misclassified points in the segmented image of CKS_FCM are significantly less than the segmented image of FLICM and NS_FCM. The region uniformity is good and the boundaries between regions are clear. This suggests that the proposed algorithm can generate satisfactory SA with good robustness.

The 6-look amplitude synthetic speckled image of size 256×256 is shown in Fig. 11(b). The segmentation results by the algorithms are shown in Fig. 11(c)–(i).

Fig. 11(c)–(f) shows the segmentation results on the 6-look amplitude synthetic speckled image using FCM_S1 FCM_S2, KFCM_S1, and KFCM_S2. All segmented images exhibit significant misclassified points. The region uniformity in the yellow region is poor. The segmentation result of FLICM on the 6-look amplitude synthetic speckled image is shown in Fig. 11(g). It can be seen that FLICM can remove a large proportion of the noise. The segmentation result of NS_FCM is shown in Fig. 11(h). The misclassified points in the segmented image of NS_FCM are less than the segmented images of FCM_S1 FCM_S2, KFCM_S1, KFCM_S2, and FLICM. The misclassified points in segmented image [Fig. 11(i)] of CKS_FCM are very small. This suggests that the proposed algorithm is superior to the compared algorithms in terms of SA.

Table VI shows the *SA* value of the proposed and the compared algorithms on the first *L*-look amplitude synthetic speckled image. The speckle looks is arranged as 1, 2, 4, and 6. The value is the mean value and standard deviation mean $\pm$ std%) for CKS_FCM with ten runs for each noise.

Table VII gives the *SA* value of the proposed and the compared algorithms on the *L*-look amplitude synthetic speckled image. The speckle looks is arranged as 1, 2, 4, and 6.

It can be seen that the *SA* of CKS_FCM is significantly higher than those of the other six compared algorithms from Tables VI and VII. The *SA* on the first 6-look amplitude synthetic speckled image is up to 99.04 ± 0.12 and the *SA* on the 6-look amplitude synthetic speckled image is up to 97.70 ± 0.14, which are higher than the other algorithms. With increasing the speckle looks, the SA increases, as expected. With the different looks of speckle noise, the proposed algorithm consistently generates better SA than the comparison algorithms.

Table VIII shows the partition coefficient v_{pc} and partition entropy v_{pe} values of the proposed and the compared algorithms on the first 6-look amplitude synthetic speckled image. The mean value and standard deviation (mean $\pm$ std) of v_{pc} and v_{pe} are given in Table VIII.

Table IX shows the partition coefficient v_{pc} and partition entropy v_{pe} values of the proposed and the compared algorithms on the 6-look amplitude synthetic speckled image. The

TABLE IX
v_{pc} AND v_{pe} ON SECOND SYNTHETIC SPECKLED IMAGE

INDEX	FCM _S1	FCM _S2	KFCM _S1	KFCM _S2	FLI CM	NS_ FCM	CKS_ FCM
v_{pc}	0.7904 ±0.002	0.7951 ±0.004	0.7401 ±0.001	0.7525 ±0.002	0.7806 ±0.001	0.7007 ±0.005	**0.8329 ±0.104**
v_{pe}	0.4037 ±0.005	0.3957 ±0.001	0.5138 ±0.002	0.4912 ±0.005	0.4288 ±0.001	0.5443 ±0.005	**0.3145 ±0.132**

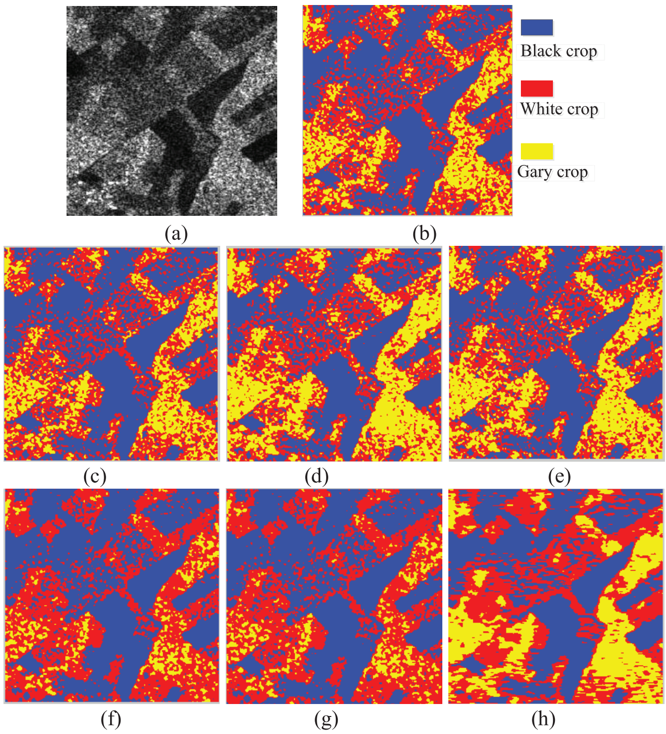

Fig. 12. Segmentation results on first real SAR image. (a) Original image. (b) FCM_S1 result. (c) FCM_S2 result. (d) KFCM_S1 result. (e) FCM_S2 result. (f) FLICM result. (g) NS_FCM result. (h) CKS_FCM result.

mean value and standard deviation (mean ± std) of v_{pc} and v_{pe} are given in Table IX.

It can be seen from Tables VIII and IX that the partition coefficient v_{pc} index of CKS_FCM is significantly closer to 1 than the other algorithms and partition entropy v_{pe} is significantly closer to 0. This suggests that the proposed algorithm outperforms the compared algorithms on this kind of test data.

E. Results on Real SAR Images

In this section, we use two real SAR images to test the effectiveness of the proposed algorithm. The first real SAR image is a four-look second ERS-2 image, shown in Fig. 12(a). It can be divided into three types of crops, visible in the image as white, gray, and black. Fig. 12(b)–(h) shows the segmentation results of the compared and proposed algorithms.

The segmentation results of the compared algorithms on the first real SAR are shown in Fig. 12(b)–(g). Fig. 12(h) shows the segmentation results generated by the proposed algorithm. The blue area, yellow area, and red area in the segmentation results represent the black crop, the gray crop, and white crop, respectively, in the original image. It can be seen that the segmentation result by FCM_S1 [Fig. 12(b)], FCM_S2 [Fig. 12(c)], KFCM_S1 [Fig. 12(d)], and KFCM_S2 [Fig. 12(e)] exhibit comparatively poor performance in terms of segmented region uniformity, and the boundaries between the white and gray crops are not well defined. FLICM [Fig. 12(f)] and NS_FCM [Fig. 12(g)] exhibit many misclassified regions in white and gray crops and many gray crops are misclassified as white crops. Overall, CKS_FCM obtains the best segmentation result, demonstrating good region uniformity, less misclassified regions, and better defined region boundaries.

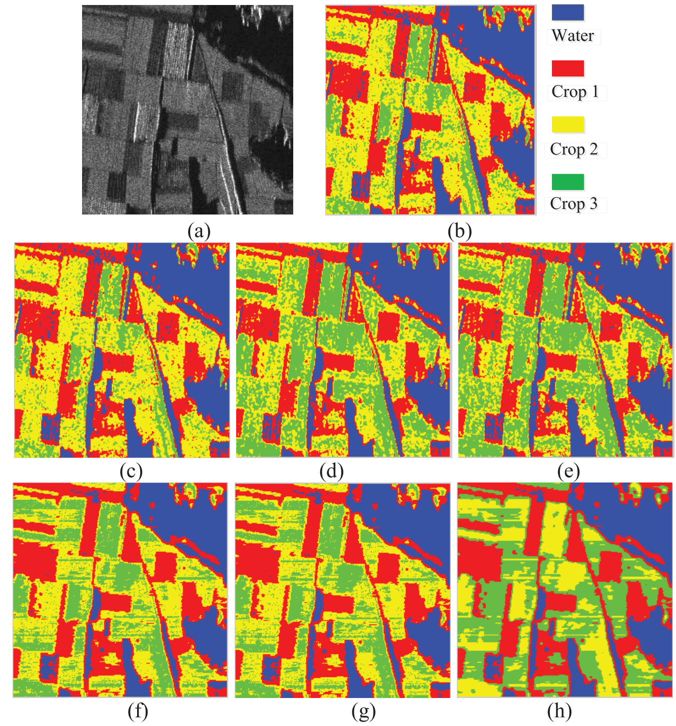

Fig. 13. Segmentation results on second real SAR image. (a) Original image. (b) FCM_S1 result. (c) FCM_S2 result. (d) KFCM_S1 result. (e) FCM_S2 result. (f) FLICM result. (g) NS_FCM result. (h) CKS_FCM result.

The second real SAR image is an eight-look SAR image of an open field in the western region of China. It can be divided into four types of land coverage: three types of crops and water. The original image is shown in Fig. 13(a) and the segmentation results by the compared algorithms and the proposed algorithm are shown in Fig. 13(b)–(h).

The segmentation results of seven different compared algorithms on the second real SAR image are shown in Fig. 13. The green, yellow, red and blue areas in the segmentation results represent the three types of crops and water, respectively. FCM_S1 [Fig. 13(b)], FCM_S2 [Fig. 13(c)], KFCM_S1 [Fig. 13(d)], and KFCM_S2 [Fig. 13(e)] misclassify the second crop regions (yellow area) and the third crop regions (green area), so the region uniformity of the segmentation results by the four comparison algorithms is poor. The boundaries in the segmentation results by FLICM [Fig. 13(f)] and NS_FCM [Fig. 13(g)] are not well defined and some regions are misclassified. In contrast, CKS_FCM [Fig. 13(h)] obtains more appropriate and satisfying segmentation results, with more defined boundaries and few misclassified regions with better region uniformity.

TABLE X
v_{pc} AND v_{pe} VALUES FOR FIRST REAL SAR IMAGE

INDEX	FCM S1	FCM S2	KFCM S1	KFCM S2	FLI CM	NS_ FCM	CKS_ FCM
v_{pc}	0.7535± 0.001	0.7606± 0.014	0.6790 ±0.022	0.6869 ±0.016	0.7830 ±0.025	0.7591 ±0.016	**0.8469 ±0.164**
v_{pe}	0.4460 ±0.013	0.4397 ±0.007	0.5765 ±0.011	0.5626 ±0.027	0.3909 ±0.013	0.4328 ±0.015	**0.3407 ±0.092**

TABLE XI
v_{pc} AND v_{pe} VALUES FOR SECOND REAL SAR IMAGE

INDEX	FCM S1	FCM S2	KFCM S1	KFCM S2	FLI CM	NS_ FCM	CKS_ FCM
v_{pc}	0.7063 ±0.012	0.7149 ±0.035	0.6651 ±0.016	0.6738 ±0.042	0.7870 ±0.023	0.6852 ±0.012	**0.8434 ±0.054**
v_{pe}	0.5564 ±0.021	0.5419 ±0.014	0.6422 ±0.041	0.6255 ±0.023	0.4178 ±0.013	0.5955 ±0.021	**0.3463 ±0.112**

Table X shows the partition coefficient v_{pc} and partition entropy v_{pe} for the proposed and the compared algorithms on the first real SAR image. For CKS_FCM, the mean value and standard deviation (mean ± std) values are shown in Table X.

Table X shows the partition coefficients v_{pc} and partition entropy v_{pe} of the proposed and the compared algorithms for the second real SAR image. For the proposed CKS_FCM algorithm, the mean and standard deviation (mean ± std) values are shown Table XI.

It can be seen from Tables X and XI that the partition coefficient v_{pc} index of CKS_FCM is closer to 1 than the other algorithms. The v_{pe} is closer to 0 than the compared algorithms. This suggests that the proposed algorithm is capable of superior segmentation on this kind of image.

Experiments on real images suggest that CKS_FCM can generate clearer segmented images, highly consistent segmented region uniformity, less misclassified regions, and better boundaries localization, as compared to the other state of the art algorithms from the literature.

F. Comparison Between Different Versions of CKS_FCM

CKS_FCM incorporates three different key components. In this section, the three different components are tested individually to evaluate the impact of these components on the algorithm's overall performance and to investigate which components play the most significant role in improving the final results. These variants are summarized as follows: "CK_FCM" denotes the CKS_FCM without spatial constraint; "CS_FCM" denotes the CKS_FCM without kernel trick; "KS_FCM" denotes CKS_FCM without immune clone. The algorithms are tested on the first synthetic image corrupted by different-level fully developed speckle noise. Speckle looks is arranged as 1, 2, 4, and 6, respectively. Table XII gives the SA of the proposed CKS_FCM and different versions of CKS_FCM on the first L-look amplitude synthetic speckled image. The SA values reported for CK_FCM, CS_FCM, and CKS_FCM show the mean value and standard deviations (mean ± std %) for 10 independent runs.

It can be seen from Table XII that the SA values of CKS_FCM consistently outperform the other comparison methods. The experimental results of CK_FCM are worse than

TABLE XII
SEGMENTATION ACCURACY ($SA\%$) FOR DIFFERENT VERSIONS OF CKS_FCM ON THE FIRST SYNTHETIC L-LOOK AMPLITUDE SYNTHETIC SPECKLED IMAGE

LOOKS	CK_FCM	CS_FCM	KS_FCM	CKS_FCM
1	61.62±1.21	84.74±1.26	91.92±0.03	92.70±1.51
2	73.92±1.29	94.21±0.68	95.28±0.09	97.26±1.76
4	82.23±1.39	94.45±1.41	96.33±0.13	98.85±1.14
6	86.61±1.33	94.49±1.46	97.43±0.10	99.04±0.46

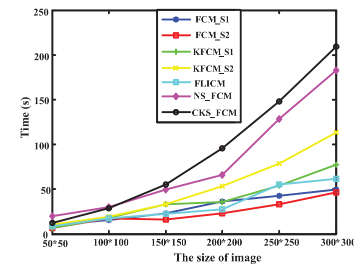

Fig. 14. Running time of the seven algorithms.

CKS_FCM when the image is corrupted by speckled noise. With the spatial constraint, CKS_FCM can take into account the image spatial information to help improve the segmentation result. The experimental results of CKS_FCM are better than those of CS_FCM, which suggests that the kernel trick is playing an important role in improving the final results. The experimental results of CKS_FCM are somewhat better than KS_FCM, suggesting that the immune clone can reduce the likelihood of converging on local optima. It appears that the spatial constraint contributes more than the kernel trick, and the immune clone contributes the smallest (but still significant) out of the three main contributions suggested in the proposed algorithm. By combining together, the three proposed improvements clearly provide an overall improvement in the performance of the proposed algorithm, as compared to other state-of-the-art methods.

G. Time Complexity of the Proposed Algorithm

In this section, we introduce Fig. 14 to illustrate the time cost of the compared algorithms as compared to the proposed algorithms on images of various different sizes. All experiments were performed on the Intel (R) Core(TM) i3 CPU M380 @ 2.53 GHz, 2G RAM, Windows 7 computer using MATLAB 2010.

As shown in Fig. 14, all algorithms can quickly generate results and the time cost is similar with the small image size. With increasing image size, the FCM_S1, FCM_S2, KFCM_S1, and KFCM_S2 algorithms are much faster than other algorithms. The proposed algorithm is time consuming comparatively, since it needs to generate the initial cluster centers by using the immune clone before fuzzy clustering, and it introduces some terms into the objective functions, so it needs to calculate each iteration step. But this drawback is compensated for by its good performance as shown above.

Analyzing the results of two groups of experiments suggests that the proposed algorithm works well. Misclassified pixels are reduced and image SA is significantly improved compared to the other six compared algorithms. The proposed algorithm performs well in terms of region uniformity and less misclassified regions in real SAR images.

IV. Conclusion

FCM algorithms often fail to achieve high SA and typically offer poor robustness against image noise. FCM is sensitive to the choices of initial cluster centers and easily becomes trapped in local optima. In order to overcome these shortcomings, this paper has proposed an improved FCM algorithm CKS_FCM. An immune clone algorithm was used to optimize the initial cluster centers, enabling convergence to the global optimum. The spatial information is added in the objective function and CKS_FCM uses a non-Euclidean distance based on kernel function to replace the Euclidean distance. This contributes to improve SA and robustness. Simulation results show that the proposed algorithm has higher SA and better robustness on both synthetic images and real SAR images. One shortcoming of the proposed work is that the number of clusters must be given *a priori* in CKS_FCM. Our ongoing and future work is investigating new ways of solving this problem.

Acknowledgment

The authors would like to express our sincere appreciation to the editors and the anonymous reviewers for their insightful comments, which have greatly helped us in improving the quality of this paper.

References

[1] X. Munoz, J. Freixenet, X. Cufi, and J. Marti, "Strategies for image segmentation combining region and boundary information," *Pattern Recognit. Lett.*, vol. 24, no. 1, pp. 375–392, 2003.

[2] J. Feng, L. Jiao, X. Zhang, M. Gong, and T. Sun, "Robust non-local fuzzy c-means algorithm with edge preservation for SAR image segmentation," *Signal Process.*, vol. 93, no. 2, pp. 487–499, Jun. 2013.

[3] J. Bezdek, L. Hall, and L. Clarke, "Review of MR image segmentation techniques using pattern recognition," *Med. Phys.*, vol. 20, pp. 1033–1048, 1993.

[4] X. Gao, R. Fu, X. Li, D. Tao, B. Zhang, and H. Yang, "Aurora image segmentation by combining patch and texture thresholding," *Comput. Vis. Image Underst.* vol. 115, no. 3, pp. 390–402, 2011.

[5] J. Kim, W. Cai, S. Eberl, and D. Feng, "Real-time volume rendering visualization of dual-modality PET/CT images with interactive fuzzy thresholding segmentation," *IEEE Trans. Inform. Technol. Biomed.*, vol. 11, no. 2, pp. 161–169, Mar. 2007.

[6] Y. Cheng and X. Li, "Adaptive image region-growing," *IEEE Trans. Image Process.*, vol. 3, no. 6, pp. 868–872, Nov. 1994.

[7] K. Strasters and J. Gerbrands, "Three-Dimensional image segmentation using a split, merge and group approach," *Pattern Recognit. Lett.*, vol. 12, no. 2 pp. 307–325, 1991.

[8] S. P. Gou, X. Zhuang, H. M. Zhu, and T. T. Yu, "Parallel sparse spectral clustering for SAR image segmentation," *IEEE J Sel. Topics Appl. Earth Observ. Remote Sens.*, vol. 6, no. 4, pp. 1949–1963, Aug. 2013.

[9] X. Descombes, M. Moctezuma, H. Maitre, and J.-P. Rudant, "Coastline detection by a Markovian segmentation on SAR images," *IEEE Trans. Signal Process.*, vol. 55, no. 1, pp. 123–132, Nov. 1996.

[10] Y. Ding, Y. Li, and W. Yu, "SAR image classification based on CRFs with integration of local label context and pairwise label compatibility," *IEEE J. Sel. Topics Appl. Earth Observ. Remote Sens.*, vol. 7, no. 1, pp. 300–306, Jan. 2014.

[11] Y. Huang and Y. C. Huang, "Segmenting SAR satellite images with the multilayer level set approach," *IEEE J. Sel. Topics Appl. Earth Observ. Remote Sens.*, vol. 4, no. 3, pp. 632–642, Sep. 2011.

[12] S. Osher and N. Paragios, *Geometric Level Set Methods in Imaging, Vision, and Graphics*. Berlin, Germany: Springer-Verlag, 2003.

[13] X. Zhang, L. Jiao, F. Liu, L. Bo, and M. Gong, "Spectral clustering ensemble applied to texture features for SAR image segmentation," *IEEE Trans. Geosci. Remote Sens.*, vol. 46, no. 7, pp. 2126–2136, Jul. 2008.

[14] Y. Zhong, S. Zhang, and L. Zhang, "Automatic fuzzy clustering based on adaptive multi-objective differential dvolution for Remote Sensing Imagery," *IEEE J. Sel. Topics Appl. Earth Observ. Remote Sens.*, vol. 6, no. 5, pp. 2390–2301, Oct. 2013.

[15] Y. Zhong, S. Zhang, and L. Zhang, "An adaptive memetic fuzzy Clustering algorithm with spatial information for Remote Sensing Imagery," *IEEE J. Sel. Topics Appl. Earth Observ. Remote Sens.*, vol. 7, no. 4, pp. 1235–1248, Apr. 2014.

[16] B. Hou, X. Zhang, Q. Ye, and Y. Zheng, "A novel method for hyperspectral image classification based on Laplacian Eigenmap pixels distribution-flow," *IEEE J. Sel. Topics Appl. Earth Observ. Remote Sens.*, vol. 6, no. 3, pp. 1602–1618, Jun. 2013.

[17] D. Pham, "An adaptive fuzzy C-means algorithm for image segmentation in the presence of intensity inhomogeneities," *Pattern Recognit. Lett.*, vol. 20, no. 1, pp. 57–68, Jan. 1999.

[18] X. Yin, S. Chen, E. Hu, and D. Zhang, "Semi-supervised clustering with metric learning: An adaptive kernel method," *Pattern Recognit. Lett.*, vol. 43, no. 4, pp. 1320–1333, Apr. 2010.

[19] J. C. Bezdek, *Pattern Recognition with Fuzzy Objective Function Algorithms*. New York, NY, USA: Plenum, 1981.

[20] J. M. Yih, "FCM algorithm based on normalized Mahalanobis distances in image clustering," in *Proc. Int. Conf. Mach. Learn. Cybern.*, 2010, vol. 5, pp. 2724–2729.

[21] R. J. Hathaway, J. C. Bezdek, and Y. Hu, "Generalized fuzzy c-means clustering strategies using norm distances," *IEEE Trans. Fuzzy Syst.*,vol. 8, no. 5, pp. 576–582, Oct. 2000.

[22] M. Ahmed, S. Yamany, N. Mohamed, A. Farag, and T. Moriarty, "A modified fuzzy C-means algorithm for bias field estimation and segmentation of MRI data," *IEEE Trans. Med. Imag.*, vol. 21, no. 3,pp. 193–199, Mar. 2002.

[23] S. Chen and D. Zhang, "Robust image segmentation using FCM with spatial constraints based on new kernel-induced distance measure," *IEEE Trans. Syst. Man Cybern.*, vol. 34, no. 4, pp. 1907–1916, Aug. 2004.

[24] L. Szilagyi, Z. Benyo, S. Szilagyii, and H. Adam, "MR brain image segmentation using an enhanced fuzzy C-means algorithm," in *Proc. IEEE 25th Annu. Int. Conf. Eng. Med. Biol. Soc. (EMBS'2013)*, 2003, pp. 17–21.

[25] W. Cai, S. Chen, and D. Zhang, "Fast and robust fuzzy C-means clustering algorithms incorporating local information for image usegmentation," *Pattern Recognit. Lett.*, vol. 40, no. 3, pp. 825–838, Mar. 2007.

[26] B. He, Y. Qiu, and Z. Li, "Similarity reasoning and similarity transformations," in *Proc. IEEE Int. Conf. Control Autom.*, Jun. 2007, pp. 1667–1671.

[27] J. Z. Wang, J. Kong, Y. H. Lu, M. Qi, and B. X. Zhang, "A modified FCM algorithm for MRI brain image segmentation using both local and non-local spatial constrains," *Comput. Med. Imag. Graph.*, vol. 32, no. 8, pp. 685–698, 2008.

[28] F. Zhao, L. C. Jiao, and H. Q. Liu, "Fuzzy c-means clustering with non local spatial information for noisy image segmentation," *Front. Comput. Sci. China*, vol. 5, no. 1, pp. 45–56, Mar. 2011.

[29] F. Zhao, L. C. Jiao, H. Q. Liu, and X. B. Gao, "A novel fuzzy clustering algorithm with non local adaptive spatial constraint for image segmentation," *Signal Process.*, vol. 91, no. 4, pp. 988–999, Apr. 2011.

[30] J. Ji and K. Wang, "A robust nonlocal fuzzy clustering algorithm with between-cluster separation measure for SAR image segmentation," *IEEE J. Sel. Topics Appl. Earth Observ. Remote Sens.*, vol. 7, no. 12, pp. 4929–4936, Oct. 2013.

[31] N. R. Pal and J. C. Bezdek, "On cluster validity for fuzzy c-means model," *IEEE Trans. Fuzzy Syst.*, vol. 3, no. 3, pp. 370–379, Aug. 1995.

[32] K. Wu and M. Yang, "Alternative C-means clustering algorithms," *Pattern Recognit.*, vol. 35, no. 10, pp. 2267–2278, 2002.

[33] S. Xie, F. Khomh, Y. Zou, and I. Keivanloo, "An empirical study on the fault-proneness of clone migration in clone genealogies," in *Proc. IEEE Conf. Software Maint. Reeng. Reverse Eng. (CSMR-WCRE)*, Feb. 2014, pp. 94–103.

[34] L. Castro and F. Zuben, "Learning and optimization using the clonal selection principle," *IEEE Trans. Evol. Comput.*, vol. 6, no. 3, pp. 239–251, Jun. 2002.

[35] A. Buades, B. Coll, and J. M. Morel, "On image denoising methods," Universitat de les Illes Balears, Mallorca, Spain, Tech. Rep. CMLA, 2004.

[36] F. Masulli and A. Schenone, "A fuzzy clustering based segmentation system as support to diagnosis in medical imaging," *Artif. Intell. Med.*, vol. 16, no. 2, pp. 129–147, 1999.

[37] S. Krinidis and V. Chatzis, "A robust fuzzy local information C-means clustering algorithm," *IEEE Trans. Image Process.*, vol. 19, no. 5, pp. 1328–1337, May 2010.

[38] K. R. Muller, S. Mika, G. Rätsch, K. Tsuda, and B. Schölkopf, "An introduction to kernel-based learning algorithms," *IEEE Trans. Neural Netw.*, vol. 12, no. 2, pp. 181–202, Mar. 2001.

[39] M. G. Gong, Y. Liang, J. Shi, W. Ma, and J. Ma, "Fuzzy C-means clustering with local information and kernel metric for image segmentation," *IEEE Trans. Image Process.*, vol. 22, no. 2, pp. 573–584, Feb. 2013.

[40] J. W. Goodman, "Some fundamental properties of speckle," *J. Opt. Soc. Amer.*, vol. 66, no. 11, pp. 1145–1150, Nov. 1976.

[41] C. Li, R. Huang, Z. Ding, J. Gatenby, D. Metaxas, and J. Gore, "A level set method for image segmentation in the presence of intensity inhomogeneities with application to MRI," *IEEE Trans. Image Process.*, vol. 20, no. 7, pp. 2007–2016, Jul. 2011.

[42] K. Chuang and H. Tzeng, "Fuzzy c-means clustering with spatial information for image segmentation," *Comput. Med. Imag. Graph.*, vol. 30, pp. 9–15, 2006.

[43] B. Hou, X. H. Zhang, X. M. Bu, and H. X. Feng, "SAR image despeckling based on nonsubsampled shearlet transform," *IEEE J. Sel. Topics Appl. Earth Observ. Remote Sens.*, vol. 5, no. 3, pp. 809–823, Jun. 2012.

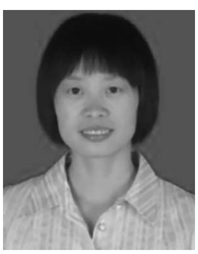

Ronghua Shang (M'09) received the B.S. degree in information and computation science and the Ph.D. degree in pattern recognition and intelligent systems from Xidian University, Xi'an, China, in 2003 and 2008, respectively.

She is currently an Associate Professor with Xidian University. Her research interests include optimization problems, evolutionary computation, image processing, and data mining.

Pingping Tian received the B.S. degree in electronic engineering from Xidian University, Xi'an, China.

Her research interests include image processing and data mining.

Licheng Jiao (SM'89) received the B.S. degree in electrical engineering from Shanghai Jiaotong University, Shanghai, China, in 1982, the M.S. degree in electrical engineering and Ph.D. degree in signal, circuit and system from Xi'an Jiaotong University, Xi'an, China, in 1984 and 1990, respectively.

From 1990 to 1991, he was a Postdoctoral Fellow with the National Key Laboratory for Radar Signal Processing, Xidian University, Xi'an, China. Since 1992, he has been a Professor with the School of Electronic Engineering, Xidian University. Currently, he is the Director of the Key Laboratory of Intelligent Perception and Image Understanding of Ministry of Education of China, Xidian University. He has charged of about 40 important scientific research projects, and published more than 20 monographs and a hundred papers in international journals and conferences. His research interests include image processing, natural computation, machine learning, and intelligent information processing.

Dr. Jiao is a member of the IEEE Xi'an Section Execution Committee and the Chairman of Awards and Recognition Committee, Vice Board Chairperson of Chinese Association of Artificial Intelligence, Councilor of Chinese Institute of Electronics, Committee Member of Chinese Committee of Neural Networks, and expert of Academic Degrees Committee of the State Council. He was selected as a member of the First level of Millions of Talents Project of China in 1996. In 2006, he was selected as an Expert with the Special Contribution of Shaanxi Province. He was the recipient of the Youth Science and Technology Award and the First Prize of Young Teacher Award of High School by the Fok Ying Tung Education Foundation, in 1992 and 2006. In 1996, he was granted by the Cross-century Specialists Fund from the Ministry of Education of China.

Rustam Stolkin (M'12) received the Bachelor's and Master's degrees in engineering science from the University of Oxford, Oxford, U.K., in 1998, and the Ph.D. degree in robotic vision from University College London, London, U.K., in 2004.

He is a Senior Birmingham Fellow with the School of Mechanical Engineering, University of Birmingham, Birmingham, U.K., researching on robotics and machine intelligence. From 2004 to 2008, he was a Research Assistant Professor with the Stevens Institute of Technology, Hoboken, NJ, USA, where he researched on sensor systems for maritime security. His research interests include science and engineering outside of robotics, as well as manipulation with robotic arms and hands, novel robotic vehicles, computer vision and other kinds of autonomous sensing.

Jie Feng received the B.S. degree from Chang'an University, Xi'an, China, in 2008. She is currently pursuing the Ph.D. degree in the laboratory of intelligent perception and image understanding from Xidian University, Xi'an, China.

Her research interests include remote sensing image processing, pattern recognition, and evolutionary computation.

Biao Hou (M'07) received the B.S. and M.S. degrees in mathematics from Northwest University, Xi'an, China, in 1996 and 1999, respectively, and the Ph.D. degree in circuits and systems from Xidian University, Xi'an, China, in 2003.

Since 2003, he has been with the Key Laboratory of Intelligent Perception and Image Understanding of the Ministry of Education, Xidian University, Xi'an, China, where he is currently a Professor. His research interests include multiscale geometric analysis and Synthetic Aperture Radar image processing.

Xiangrong Zhang (M'06) received B.S. and M.S. degrees in computer science and technology from Xidian University, Xi'an, China, in 1999 and 2003, respectively and the Ph.D. degree in pattern recognition and intelligent system from Xidian University, in 2006.

She is a Professor in the School of Electronic Engineering, Xidian University. Her research interests include action recognition and machine learning.